BIOCHEMISTRY
including biophysical chemistry & molecular biology

Article

pubs.acs.org/biochemistry

Differential Pharmacological Activity of JN403 between α7 and Muscle Nicotinic Acetylcholine Receptors

Hugo R. Arias,*[,†] Maria Jose De Rosa,[‡] Ignacio Bergé,[‡] Dominik Feuerbach,[§] and Cecilia Bouzat*[,‡]

[†]Department of Medical Education, California Northstate University College of Medicine, Elk Grove, California 95757, United States
[‡]Instituto de Investigaciones Bioquímicas de Bahía Blanca, UNS-CONICET, 8000 Bahia Blanca, Argentina
[§]Novartis Institutes for Biomedical Research, CH-4002 Basel, Switzerland

ABSTRACT: The differential action of the novel agonist JN403 at neuronal α7 and muscle nicotinic receptors (AChRs) was explored by using a combination of functional and structural approaches. Single-channel recordings reveal that JN403 is a potent agonist of α7 but a very low-efficacy agonist of muscle AChRs. JN403 elicits detectable openings of α7 and muscle AChRs at concentrations ∼1000-fold lower and ∼20-fold higher, respectively, than that for ACh. Single-channel activity elicited by JN403 is very similar to that elicited by ACh in α7 but profoundly different in muscle AChRs, where openings are brief and infrequent and do not appear in clusters at any concentration. JN403 elicits single-channel activity of muscle AChRs lacking the ε subunit, with opening events being more frequent and prolonged than those of wild-type AChRs. This finding is in line with the molecular docking studies predicting that JN403 may form a hydrogen bond required for potent activation at the α−δ but not at the α−ε binding site. JN403 does not elicit detectable Ca^{2+} influx in muscle AChRs but inhibits (±)-epibatidine-elicited influx mainly by a noncompetitive mechanism. Such inhibition is compatible with single-channel recordings revealing that JN403 produces open-channel blockade and early termination of ACh-elicited clusters, and it is therefore also a potent desensitizing enhancer of muscle AChRs. The latter mechanism is supported by the JN403-induced increase in the level of binding of [^{3}H]cytisine and [^{3}H]TCP to resting AChRs. Elucidation of the differences in activity of JN403 between neuronal α7 and muscle AChRs provides further insights into mechanisms underlying selectivity for α7 AChRs.

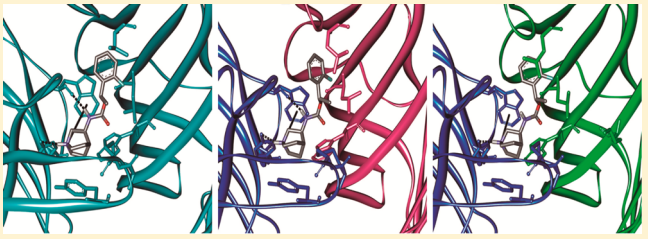

Nicotinic acetylcholine receptors (AChRs) are members of the Cys-loop ligand-gated ion-channel superfamily that also includes glycine, type 3 serotonin, and type A and C GABA receptors (reviewed in refs 1−6). α7 AChRs are homomeric receptors that can be pharmacologically and functionally distinguished from other neuronal AChR subtypes because they have a high affinity for the competitive antagonist α-bungarotoxin (α-BTx), a low affinity for the agonist (−)-nicotine, and a high Ca^{2+}/Na^{+} permeability ratio, they can be fully activated by choline, and they desensitize very rapidly. Interestingly, muscle and α7 AChRs share its high affinity for α-BTx. α7 AChRs are some of the most prominent receptors in the brain and are implicated in diseases such as Alzheimer's disease, schizophrenia, drug addiction, neuronal and peripheral inflammation, and cancer, whereas muscle AChRs are confined at postsynaptic locations in muscle fibers and are mainly implicated in Myasthenia gravis and myasthenic syndromes (reviewed in refs 2, 3, and 7). In this regard, a better understanding of the interaction of agonists with AChRs, and in particular with α7, is crucial to the development of more specific and, consequently, safer ligands for different therapeutic purposes. JN403 [(*S*)-(1-azabicyclo[2.2.2]oct-3-yl)carbamic acid (*S*)-1-(2-fluorophenyl)ethyl ester] is a partial but potent agonist of α7 AChR[8,9] that improves cognition and sensory gating deficits and decreases pain, epileptic seizures, and anxiety.[10] Thus, deciphering the molecular basis of its selectivity among members of the nicotinic receptor family is of great significance. To this end, the interaction of JN403 with neuronal α7 AChRs was compared to that for muscle AChRs by patch-clamp, radioligand binding, Ca^{2+} influx, and molecular docking studies.

EXPERIMENTAL PROCEDURES

Materials. [^{3}H]Cytisine (35.6 Ci/mmol) and [^{3}H]TCP [piperidyl-3,4-^{3}H(*N*)]-{*N*-[1-(2-thienyl)cyclohexyl]-3,4-piperidine} (45 Ci/mmol) were obtained from PerkinElmer Life Sciences Products, Inc. (Boston, MA) and stored in ethanol at −20 °C. Carbamylcholine chloride (CCh), acetylcholine chloride (ACh), polyethylenimine, and proadifen hydrochloride were purchased from Sigma Chemical Co. (St. Louis, MO). Phencyclidine hydrochloride (PCP) was obtained from the National Institute on Drug Abuse (National Institutes of Health, Baltimore, MD). (±)-Epibatidine hydrochloride was obtained from Tocris Bioscience (Ellisville, MO). Fetal bovine serum (FBS) and trypsin/EDTA were purchased form Gibco BRL (Paisley, U.K.). JN403 was synthesized as previously described.[8] Salts were of analytical grade.

Received: May 17, 2013
Revised: October 22, 2013

   dx.doi.org/10.1021/bi4012572 | *Biochemistry* XXXX, XXX, XXX−XXX

Ca^{2+} Influx Measurements in TE671-$\alpha\beta\gamma\delta$ and HAM293-$\alpha\beta\varepsilon\delta$ Cells. Ca^{2+} influx experiments were performed in TE671 and HAM293 cells expressing human embryonic (i.e., $\alpha\beta\gamma\delta$) and adult (i.e., $\alpha\beta\varepsilon\delta$) muscle AChRs, respectively, as previously described.[11,12] Briefly, TE671-$\alpha\beta\gamma\delta$ and HAM293-$\alpha\beta\varepsilon\delta$ cells were seeded 72 h prior to the experiment on black 96-well plates (Costar) at a density of 5×10^4 cells per well and incubated at 37 °C; 16−24 h before the experiment, the medium was changed to 1% FBS in a HEPES-buffered salt solution (HBSS) [130 mM NaCl, 5.4 mM KCl, 2 mM $CaCl_2$, 0.8 mM $MgSO_4$, 0.9 mM NaH_2PO_4, 25 mM glucose, and 20 mM HEPES (pH 7.4)]. On the day of the experiment, the medium was replaced with 100 μL of HBSS and 1% FBS containing 2 μM Fluo-4 (Molecular Probes, Eugene, OR) in the presence of 2.5 mM probenecid (Sigma, Buchs, Switzerland). The cells were then incubated at 37 °C for 1 h. Plates were washed twice with HBSS/NMDG buffer [130 mM *N*-methyl-D-glucamine, 4.5 mM KCl, 2 mM $CaCl_2$, 0.8 mM $MgSO_4$, 0.9 mM KH_2PO_4, 25 mM glucose, and 20 mM HEPES (pH 7.4)] and finally refilled with 100 μL of HBSS/NMDG buffer containing different concentrations of JN403 and preincubated for 5 min. Plates were then placed in the cell plate stage of the fluorescent imaging plate reader (FLIPR) (Molecular Devices, Sunnyvale, CA). A baseline consisting of five measurements of 0.4 s each was recorded. (±)-Epibatidine (1 μM) was then added from the agonist plate to the cell plate using the 96-tip pipettor at the same time fluorescence recordings were being taken for a total of 3 min. To determine the inhibitory mechanism for JN403, additional experiments were performed by preincubating the cells with 30, 100, and 300 μM JN403 before the (±)-epibatidine-induced Ca^{2+} influx determinations. To determine the agonistic activity of JN403, the fluorescence was recorded after the cells were stimulated by increasing concentrations of JN403. The laser excitation and emission wavelengths are 488 and 510 nm, respectively, at 1 W, with a CCD camera opening of 0.4 s.

Patch-Clamp Recordings from BOSC 23 Cells. BOSC 23 cells were transfected with mouse α, β, and δ subunits together with (adult muscle AChR) or without ($\alpha\beta\delta$ AChR) the ε subunit, or with α7 and Ric-3, for expression of α7 AChRs, as previously described.[13−16] A plasmid encoding green fluorescent protein was included in all transfections to allow identification of transfected cells under fluorescence optics. Cells were used for single-channel measurements 1 or 2 days after transfection. Single-channel recordings were performed in the cell-attached configuration[17] at a membrane potential of −70 mV and 20 °C. The bath and pipet solutions contained 142 mM KCl, 5.4 mM NaCl, 1.8 mM $CaCl_2$, 1.7 mM $MgCl_2$, and 10 mM HEPES (pH 7.4). Single-channel currents were recorded using an Axopatch 200 B patch-clamp amplifier (Molecular Devices Corp.), digitized at 100 kHz, and detected by the half-amplitude threshold criterion using TAC version 4.0.10 (Bruxton Corp.) at a final bandwidth of 10 kHz.[14] Open- and closed-time histograms were constructed with an imposed dead time of 30 μs and fit to the sum of exponential functions by maximum likelihood using TACFit (Bruxton Corp.).

Radioligand Binding Experiments. The effect of JN403 on the binding of the agonist [^{3}H]cytisine and of the noncompetitive antagonist [^{3}H]TCP to *Torpedo* AChR native membranes was studied as previously described.[11,12] In this regard, AChR membranes (0.3 μM) were suspended in binding saline buffer [50 mM Tris-HCl, 120 mM NaCl, 5 mM KCl, 2 mM $CaCl_2$, and 1 mM $MgCl_2$ (pH 7.4)] with 8.6 nM [^{3}H]cytisine or 19 nM [^{3}H]TCP and preincubated for 30 min at room temperature in the presence of 1 mM CCh ([^{3}H]TCP experiments) or 200 μM proadifen ([^{3}H]cytisine experiments) (AChRs are mainly in the desensitized state), or in the absence of any ligand (AChRs are mainly in the resting but activatable state). Nonspecific binding was assessed in the presence of 1 mM CCh ([^{3}H]cytisine experiments) or 100 μM PCP ([^{3}H]TCP experiments). The total volume was divided into aliquots, and increasing concentrations of JN403 were added to each tube and incubated for 2 h at room temperature. AChR-bound radioligand was then separated from free radioligand by a filtration assay using a 48-sample harvester system with GF/B Whatman filters (Brandel Inc., Gaithersburg, MD), previously soaked with 0.5% polyethylenimine for 30 min. The membrane-containing filters were transferred to scintillation vials with 3 mL of Bio-Safe II (Research Product International Corp., Mount Prospect, IL), and the radioactivity was determined using a Beckman LS6500 scintillation counter (Beckman Coulter, Inc., Fullerton, CA). The concentration−response data were curve-fitted by nonlinear least-squares analysis using Prism (GraphPad Software, San Diego, CA), and the corresponding IC_{50} and n_H (Hill coefficient) values were calculated. The observed IC_{50} values were transformed into inhibition constant (K_i) values using the following relationship:[18]

$$K_i = IC_{50}/[1 + [L_{50}]/K_d^{ligand} + 2([L_{50}] - [L])/[L]] \quad (1)$$

where $[L_{50}]$ is the free concentration of the radioligand (e.g., [^{3}H]cytisine or [^{3}H]TCP) at the competitor concentration producing 50% inhibition (i.e., IC_{50}), [L] is the free concentration of the radioligand in the absence of the competitor, and K_d^{ligand} is the dissociation constant for [^{3}H]cytisine (0.45 μM)[12] and [^{3}H]TCP (0.25 μM)[19] when the receptor is in the desensitized state. The K_i and n_H values are summarized in Table 2.

Molecular Docking. Homology modeling of the extracellular portion from the $\alpha\beta\varepsilon\delta$ and α7 AChRs was based on the crystal structure of the acetylcholine binding protein [AChBP; Protein Data Bank (PDB) entry 1I9B] as described previously.[9] Multiple-sequence alignment between the AChBP and the extracellular domains of the α, β, δ, and ε subunits was performed by using CLUSTALW, and modeling was conducted using Modeler version 9.11.[20] Because loop F at the ε and δ subunits is longer than that at the AChBP,[21] its modeling is not reliable; therefore, this loop was not included in the analysis. Because the two α subunits have the same amino acid sequence, symmetry constraints were imposed on the Cα atoms of both α subunits. Ten models were constructed, and the one with the highest MODELER scores and the smallest percentage of amino acids in the disallowed region of the Ramachandran plot was selected for docking studies. The protonated form of JN403 was docked to the agonist binding sites located at the α7−α7, α−δ, and α−ε interfaces using AutoDock version 4.3.[22] The ligand binding site was defined as being within 20 Å of W149.[21] One hundred genetic algorithm runs were performed for each condition. Clustering of the results was done with AutoDock based on a root-mean-square deviation cutoff of 2.0 Å.

RESULTS

JN403 Inhibits (±)-Epibatidine-Induced Ca^{2+} Influx in TE671-$\alpha\beta\gamma\delta$ and HAM293-$\alpha\beta\varepsilon\delta$ Cells with Low Potency. The activation of both muscle embryonic ($\alpha\beta\gamma\delta$) (Figure 1A) and adult ($\alpha\beta\varepsilon\delta$) (Figure 1B) AChRs was first determined by

dx.doi.org/10.1021/bi4012572 | *Biochemistry* XXXX, XXX, XXX−XXX

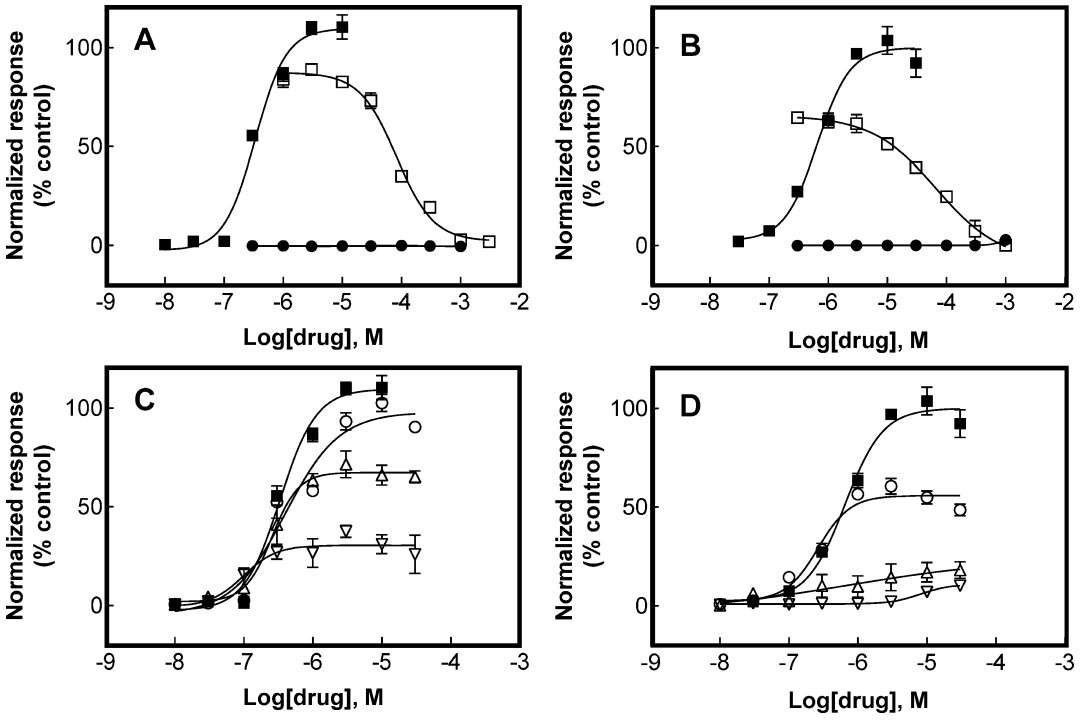

Figure 1. Effect of JN403 on TE671-$\alpha\beta\gamma\delta$ and HAM293-$\alpha\beta\varepsilon\delta$ cells using Ca^{2+} influx measurements. (A and B) Increased concentrations of (±)-epibatidine (■) enhance Ca^{2+} influx, whereas increased concentrations of JN403 (●) do not enhance intracellular calcium in the tested concentration range (≤1 mM). The antagonistic effect of JN403 was investigated after the cells had been pretreated (5 min) with different concentrations of JN403 followed by activation of $\alpha\beta\gamma\delta$ (A) and $\alpha\beta\varepsilon\delta$ (B) AChRs with 1 μM (±)-epibatidine (□). Shown are representative plots of 17 (A, ■), 3 (B, ■); 3 (A and B, ●), 8 (A, □), and 3 (B, □) experiments, where the error bars represent the standard deviation (SD). The ligand response was normalized to the maximal (±)-epibatidine response, which was set to 100%. The calculated EC_{50}, IC_{50}, and n_H values are summarized in Table 1. (C and D) Pretreatment with 30 (○), 100 (△), or 300 μM JN403 (▽) (n = 3) inhibits (±)-epibatidine-elicited $\alpha\beta\gamma\delta$ (C) and $\alpha\beta\varepsilon\delta$ (D) AChR activation (■) in a dose-dependent and noncompetitive manner.

assessing the fluorescence change elicited by (±)-epibatidine-induced Ca^{2+} influx. (±)-Epibatidine activates embryonic AChRs with a potency >2-fold higher than that for adult AChRs (Table 1). The observed potency for these AChRs is consistent with previous determinations.[11,12] In contrast, JN403 does not produce any detectable response from either AChR in the tested concentration range (≤1 mM). Moreover, the drug inhibits (±)-epibatidine-induced Ca^{2+} influx in a concentration-dependent (Figure 1A,B) and noncompetitive (Figure 1C,D) manner. The calculated IC_{50} values indicate that JN403 inhibits $\alpha\beta\varepsilon\delta$ AChRs with a potency 1.8-fold higher than that for $\alpha\beta\gamma\delta$ AChRs (Table 1). The observed n_H values are higher than unity (Table 1), suggesting that (±)-epibatidine and JN403 interact with the AChR in a cooperative manner.

Table 1. Activation Potencies (EC_{50}) of (±)-Epibatidine and Inhibitory Potencies (IC_{50}) of JN403 on Human Embryonic and Adult Muscle AChRs Obtained by Ca^{2+} Influx Measurements

AChR subtype	EC_{50} (nM)	n_H[c]	IC_{50} (μM)	n_H[c]
embryonic ($\alpha\beta\gamma\delta$)[a]	263 ± 37	1.23 ± 0.06	154 ± 35	1.31 ± 0.10
adult ($\alpha\beta\varepsilon\delta$)[b]	602 ± 41	1.62 ± 0.06	86 ± 26	2.26 ± 1.02

[a]Values obtained from Figure 1A. [b]Values obtained from Figure 1B. [c]Hill coefficients.

Interaction of JN403 with *Torpedo* AChRs in Different Conformational States. To explore in more detail the action for JN403 at muscle AChRs, we took advantage of the fact that the *Torpedo* AChR (embryonic muscle subtype) can be manipulated *in vitro* to shift its conformation to the resting or desensitized state, which allows radioligand binding assays to be performed in each conformational state. The experiments in the desensitized state (i.e., in the presence of proadifen) show that JN403 inhibits [^{3}H]cytisine binding with a low affinity [K_i = 112 ± 15 μM (Table 2)]. In contrast, JN403 enhances the binding of [^{3}H]cytisine to AChRs in the resting state (Figure 2 and Table 2). This suggests that JN403 may act through a site different from the orthosteric sites and consequently by a different mechanism. An alternative mechanism can be addressed on the basis of the fact that the AChR membrane suspension contains an excess of agonist

Table 2. Interaction of JN403 with the Agonist and Luminal Binding Sites of *Torpedo* AChRs in Different Conformational States

	desensitized state		resting but activatable state	
radioligand	K_i (μM)[a]	n_H[b]	apparent EC_{50} (μM)[c]	apparent n_H[b]
[^{3}H]cytisine	112 ± 15	0.77 ± 0.08	23 ± 12	0.89 ± 0.28
[^{3}H]TCP	266 ± 14	0.96 ± 0.05	35 ± 15	0.94 ± 0.25

[a]K_i values for the desensitized AChR were determined in the presence of proadifen [[^{3}H]cytisine experiments (Figure 2)] and CCh [[^{3}H]TCP experiments (Figure 3)], according to eq 1. [b]Hill coefficients. [c]Apparent EC_{50} values for the AChR in the resting but activatable state were calculated in the absence of any additional ligand, according to eq 1.

dx.doi.org/10.1021/bi4012572 | *Biochemistry* XXXX, XXX, XXX−XXX

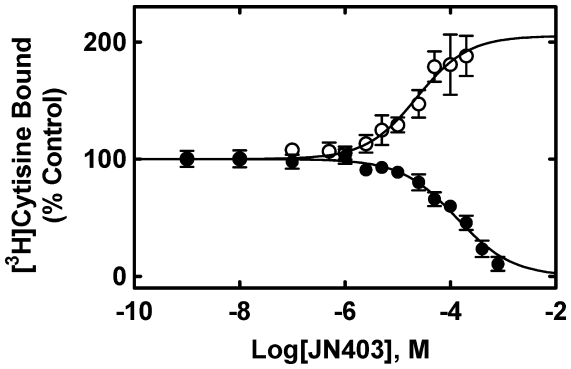

Figure 2. JN403-induced modulation of the binding of [^{3}H]cytisine to *Torpedo* AChRs in different conformational states. *Torpedo* AChR membranes (0.3 μM) were preincubated (30 min) with 8.6 nM [^{3}H]cytisine in the absence (○) (AChRs are in the resting but activatable state) or presence of 200 μM proadifen (●) (AChRs are mainly in the desensitized state) and then equilibrated (1 h) with increasing concentrations of JN403. Nonspecific binding was assessed at 1 mM CCh. Each plot is the combination of two separate experiments each performed in triplicate, where the error bars correspond to the SD. From these plots, the IC_{50}, apparent EC_{50}, and n_H values were obtained by nonlinear least-squares fit. The IC_{50} values were transformed into K_i values using eq 1. The data are summarized in Table 2.

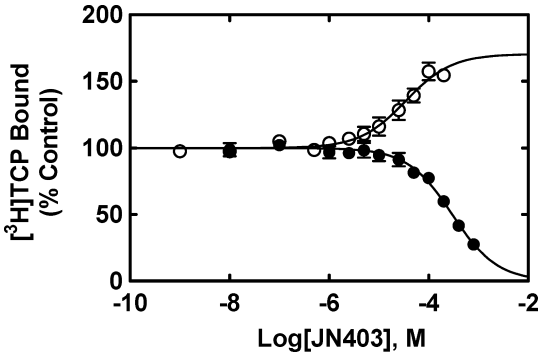

Figure 3. JN403-induced modulation of the binding of [^{3}H]TCP to *Torpedo* AChRs in different conformational states. *Torpedo* AChR membranes (0.3 μM) were preincubated (30 min) with 19 nM [^{3}H]TCP in the absence (○) (AChRs are in the resting but activatable state) or presence of 1 mM CCh (●) (AChRs are mainly in the desensitized state) and then equilibrated (1 h) with increasing concentrations of JN403. Nonspecific binding was assessed at 100 μM PCP. Each plot is the combination of two or three separated experiments each performed in triplicate, where the error bars correspond to the SD. From these plots, the IC_{50}, apparent EC_{50}, and n_H values were obtained by a nonlinear least-squares fit. The IC_{50} values were transformed into K_i values using eq 1. The data are summarized in Table 2.

binding sites (0.6 μM) compared with the initial concentration of [^{3}H]cytisine used (8.6 nM; similar results were obtained at 5.4 nM). Because the cytisine K_i in the resting state is 1.6 μM,[12] only a small fraction of AChRs is initially labeled with [^{3}H]cytisine. Considering n_H = 1, a fractional occupancy of ~0.006 is calculated for [^{3}H]cytisine bound to resting AChRs. Thus, if the AChR is shifted to its high-affinity (i.e., desensitized) state, an increase in the AChR-bound [^{3}H]cytisine fraction can be expected. Considering that the cytisine K_i in the desensitized state is 0.45 μM,[12] a fractional occupancy of ~0.019 for [^{3}H]cytisine bound to desensitized AChRs is obtained, which corresponds to an ~3-fold increase in fractional occupancy. Coincident with this calculation, our results indicate ~2-fold enhanced binding (see Figure 2). Thus, it could be possible that when JN403 binds to an allosteric site(s), AChRs become desensitized, the affinity of [^{3}H]cytisine is increased, and subsequently a larger fraction of AChR-bound [^{3}H]cytisine is observed. To quantify the enhanced binding, we calculated the drug concentration required to produce a 50% increase in the level of [^{3}H]cytisine binding (i.e., apparent EC_{50} in Table 2), which correlates with its desensitizing potency.

To determine whether JN403 binds to a noncompetitive antagonist site in muscle AChRs, [^{3}H]TCP binding experiments were performed (Figure 3). [^{3}H]TCP is a high-affinity noncompetitive antagonist of *Torpedo* and muscle AChRs, and its luminal binding site has been located within the ion channel between the threonine (position 2′) and valine (position 13′) rings (reviewed in ref 23). JN403 enhances [^{3}H]TCP binding when the AChR is in the resting but activatable state (i.e., no other ligand present) (Figure 3 and Table 2). These results indicate that this drug does not bind to the TCP binding site when the receptor is in the resting state. Considering that the affinity of [^{3}H]TCP for the desensitized AChR (0.25 μM)[19] is higher than that for the resting AChR (0.83 μM),[24] our results support the idea that after JN403 binding, AChR becomes desensitized and therefore the TCP affinity increases, resulting in a larger AChR-bound [^{3}H]TCP fraction (Figure 3). This mechanism is in agreement with the [^{3}H]cytisine results in the resting state (Figure 2). In fact, the desensitizing potency (i.e., apparent EC_{50} values) for JN403 obtained from the [^{3}H]TCP experiments is similar to that obtained from the [^{3}H]cytisine experiments (Table 2). On the other hand, the results in the desensitized state (i.e., in the presence of CCh) indicate that JN403 binds to the [^{3}H]TCP site with a very low affinity [K_i = 266 ± 14 μM (Table 2)].

Although a potential JN403 depletion can occur because of the high levels of the AChR-bound ligand, it is evident that JN403 produces two totally opposite effects depending on the conformational state of the AChR (Figures 2 and 3).

JN403 Acts as a Very Low-Efficacy Agonist of Adult Muscle AChRs. To gain further insight into the action of JN403 at muscle AChRs, we evaluated its action at the single-channel level. Opening events from cells expressing $\alpha\beta\delta\varepsilon$ AChRs are detected in cell-attached patches in the presence of 10 μM JN403 in the pipet solution (Figure 4A), indicating that this drug is capable of activating muscle AChRs with very low efficacy. At low concentrations (1 μM), opening events appear very infrequently, in contrast to what is observed in the presence of 1 μM ACh.[14] Single-channel activity also differs significantly from that observed in the presence of ACh. Openings are very infrequent, appear as isolated events, and are briefer than those elicited by ACh (Figure 4).

At ACh concentrations of >10 μM, single-channel openings appear to be grouped in well-defined clusters (Figure 4).[14] A cluster results from the activity of a single receptor, which recovers from long-lived desensitization and begins a series of transitions through open and closed states. At the end of the cluster, the receptor re-enters the desensitized state.[14] In contrast, when JN403 is used, clusters are not detected even at concentrations as high as 1 mM (Figure 4A).

Open-time histograms of channels activated by 10 μM JN403 can be well fitted by a single component whose duration is 155 ± 16 μs (n = 3) (Figure 4A), which is ~6-fold briefer than

dx.doi.org/10.1021/bi4012572 | *Biochemistry* XXXX, XXX, XXX−XXX

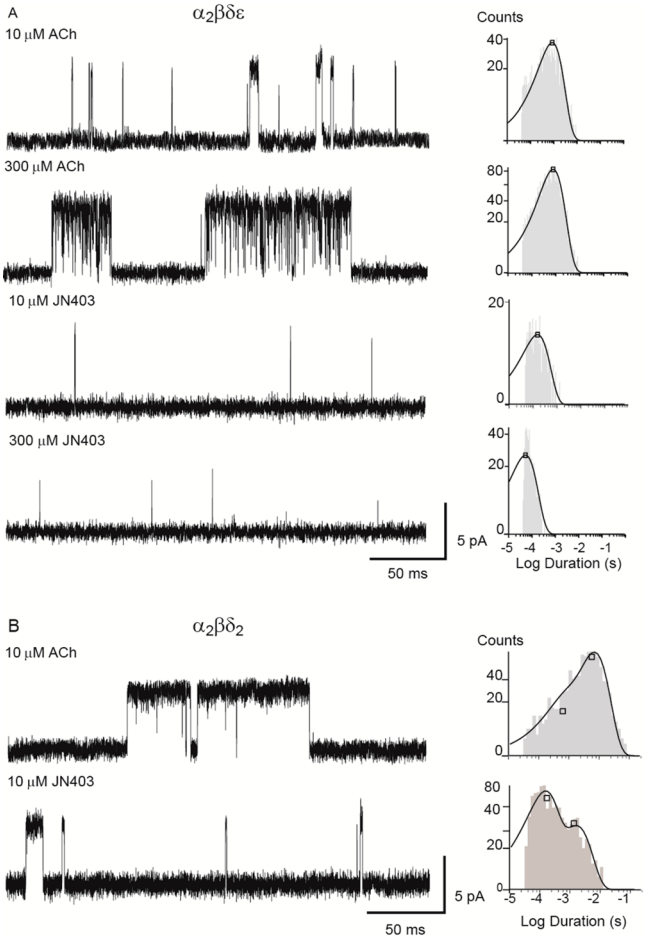

Figure 4. (A) Channel traces (left) corresponding to adult muscle AChRs ($\alpha\beta\delta\varepsilon$) activated by ACh and JN403. Single-channel activity recorded for each agonist at 10 and 300 μM. Open-time histograms (right) corresponding to each condition. (B) Channel traces (left) corresponding to $\alpha\beta\delta$ AChRs activated by 10 μM ACh and JN403. Open-time histograms (right) corresponding to each condition. Current traces are displayed at a bandwidth of 9 kHz with openings as upward deflections. The membrane potential was −70 mV.

that of ACh-activated channels.[14] In addition, increasing JN403 concentrations are accompanied by a significant reduction in the mean open time, for instance, 104 ± 6 μs at 100 μM, 69 ± 15 μs at 300 μM, and 40 ± 3 μs at 1 mM. Such concentration-dependent decreases may be explained by open-channel blockade induced by the agonist.

The simplest linear kinetic scheme that describes the inhibitory action of an open-channel blocker is

$$C \leftrightarrow O \underset{k_{-b}}{\overset{k_{+b}[B]}{\longleftrightarrow}} OB \qquad \text{(Scheme 1)}$$

where C represents the closed (resting) state, O the open (activated) state, and OB the blocked state. We calculated the association rate constant of the blocking reaction (k_{+b}) from the slope of the linear regression of the relationship between the reciprocal of the mean open time and JN403 concentration, thus resulting in an estimated k_{+b} value for JN403 of 1.8 × 10^7 M^{-1} s^{-1} (−70 mV). This set of results indicates that JN403 acts on muscle AChRs as a low-efficacy agonist and potent blocker.

To gain more insights into the process of JN403-induced activation, the importance of the $\alpha-\delta$ binding site interface was evaluated by studying the activation of AChRs lacking the ε subunit. In the absence of this subunit, AChRs contain two $\alpha-\delta$ binding site interfaces instead of one $\alpha-\delta$ and one $\alpha-\varepsilon$ interface as in wild-type AChRs. These receptors express well in cells and are activated by ACh. However, ACh-elicited openings show prolonged durations with respect to those of wild-type AChRs (Figure 4B).[13] The mean duration of the slowest open component for ACh-activated channels is 8.1 ± 1.8 ms instead of ∼1 ms for wild-type AChRs. JN403 (10 μM) also elicits single-channel currents from $\alpha\beta\delta$ receptors (Figure 4B), indicating that this drug is capable of activating AChRs through the $\alpha-\delta$ interface. In agreement with ACh-elicited channels, open durations are more prolonged than in wild-type AChRs, and open-time histograms exhibit an additional slower component whose duration is 1.6 ± 0.1 ms [relative area of 0.35 ± 0.06 (n = 3)].

Effect of JN403 on ACh-Activated Muscle AChRs. To explore in more detail the action of JN403, we studied its effect on single channels activated by 100 μM ACh. At 100 μM ACh, channel activation appears in well-defined clusters (Figure 5). In the absence of JN403, open-time histograms are fit by a main component of 1.04 ± 0.02 ms.[14] In the presence of 1 μM JN403, the mean open time of 100 μM ACh-activated channels is not affected [1.03 ± 0.29 ms (n = 3)] (Figure 5), whereas it

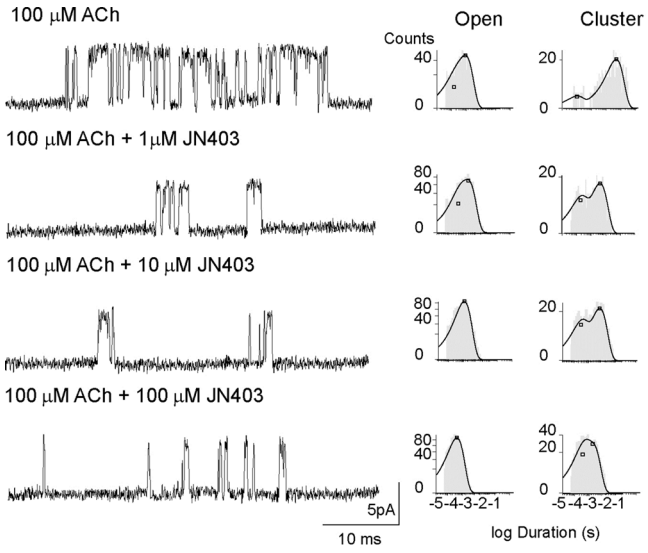

Figure 5. Combined action of ACh and JN403 on adult muscle AChRs. Single-channel recordings were performed in the presence of 100 μM ACh and different JN403 concentrations. Current traces (left) are displayed at a bandwidth of 9 kHz with openings as upward deflections. The membrane potential was −70 mV. Representative open-time and cluster-duration histograms (right) corresponding to each condition.

decreases 2- and 4-fold when the JN403 concentration is increased to 10 and 100 μM, respectively. These results suggest that JN403 produces open-channel blockade of ACh-activated channels. In addition, significant changes in cluster duration are observed in the presence of JN403 (Figure 5). The mean cluster duration of muscle AChR channels activated by 100 μM ACh is 46.4 ± 8.7 ms. This duration decreases to 5.1 ± 3.1, 3.8 ± 0.6, and 0.8 ± 0.2 ms in the presence of 1, 10, and 100 μM JN403, respectively. The profound decrease in cluster duration can be explained by the increase in desensitization rate.[25] The fact that at 1 μM JN403 the cluster duration decreases significantly but the mean open time is not affected suggests that

dx.doi.org/10.1021/bi4012572 | Biochemistry XXXX, XXX, XXX−XXX

at low concentrations the drug enhances desensitization whereas at higher concentrations (≥10 uM) the blocking effect becomes more evident.

JN403 Activates α7 AChR at a Lower Concentration Than ACh. Single channels from α7 AChRs are detected in cell-attached patches in the presence of 10 μM ACh (Figure 6)

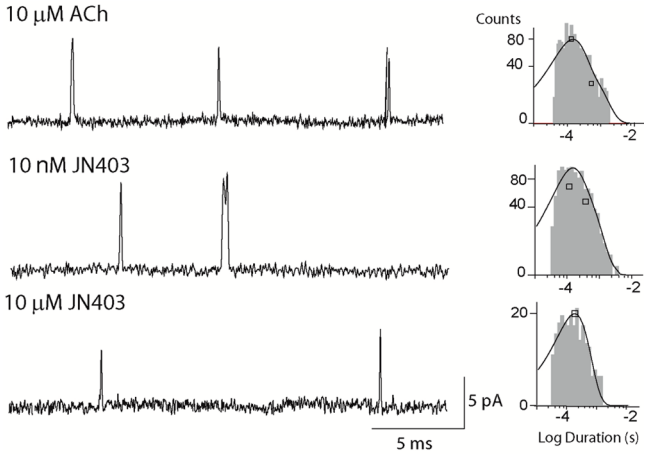

Figure 6. Channel traces corresponding to α7 AChRs activated by ACh or JN403. Single-α7 channels (left) are displayed at a bandwidth of 9 kHz with openings as upward deflections. The membrane potential was −70 mV. Representative open-time histograms (right) corresponding to each condition.

(see also ref 26). Channel activity appears as single brief pulses flanked by long closed periods, or less often as a few openings in quick succession (i.e., bursts). At −70 mV, opening events show maximal amplitudes of ∼10 pA. However, lower-amplitude openings, which result from the lack of full amplitude resolution due to the brief open durations, are observed (Figure 6). Open-time distributions are described well by the sum of two exponential components whose mean durations are 50 ± 10 μs (relative area of 0.70 ± 0.05) and 284 ± 64 μs (Figure 6) (see also ref 26).

Similar channel activity is detected from single-channel recordings when JN403 is used as the agonist (Figure 6). However, channel openings can be detected at concentrations as low as 5 nM. Given that ∼10 μM ACh is about the minimal concentration required for detecting α7 channels,[26] this finding indicates that JN403 is remarkably more potent than the endogenous neurotransmitter. As expected, JN403-activated channels exhibit amplitudes identical to those elicited by ACh (Figure 6). The open-time histograms also show two open components whose mean durations are 117 ± 24 μs (relative area of 0.73 ± 0.05) and 380 ± 66 μs, similar to those of ACh-activated channels. At concentrations of ≥10 μM, single-channel activity is very infrequent, and only the brief open component is observed (mean duration of 112 ± 35 μs at 10 μM). Although the infrequent and very brief openings do not allow a detailed characterization of open and closed times in this concentration range, the absence of the slower open component could be explained by open-channel blockade or an increased level of desensitization mediated by JN403.[26] Any of these mechanisms or the combination of these mechanisms may account for the observed partial agonistic activity of JN403 in *in vitro* systems of recombinant α7 AChRs.[8]

Molecular Docking of JN403 into the α7−α7, α−ε, and α−δ Interfaces. To gain further insight into the differences in JN403 interaction between α7 and muscle AChR binding sites, we performed *in silico* studies. Molecular docking of JN403 at the α−ε and α−δ interfaces (Figure 7B,C) was compared to that described for the α7 AChR (Figure 7A).[9] In the α7 orthosteric sites, the ammonium group of JN403

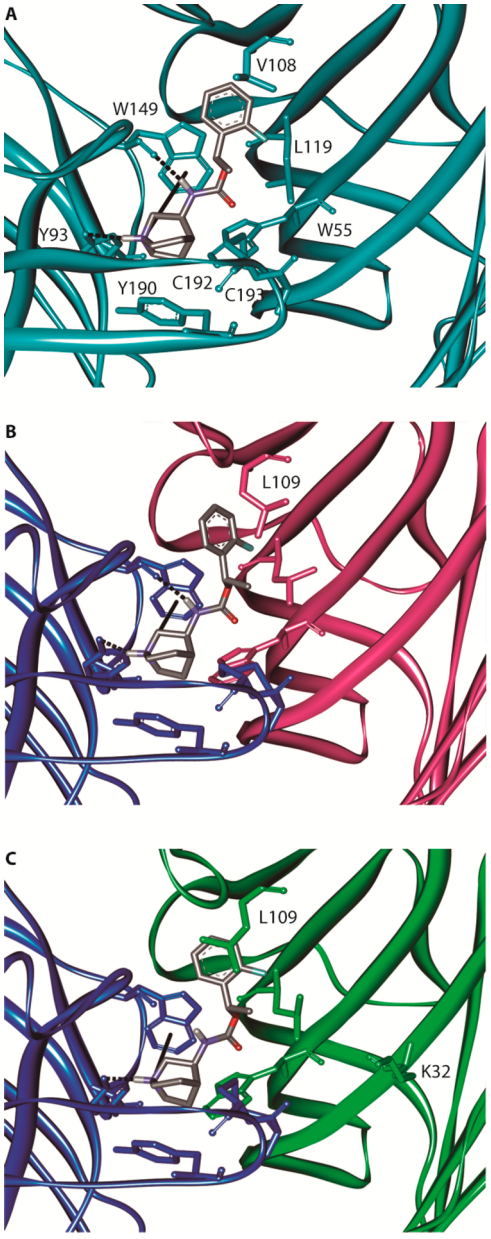

Figure 7. Molecular docking of JN403 to α7−α7, α−δ, and α−ε interfaces. Homology models of α7−α7 (A), α−δ (B), and α−ε (C) interfaces were generated using the structure of the AChBP (PDB entry 1I9B) as described in Experimental Procedures. The subunits and the corresponding residues are colored cyan (α7), blue (α), pink (δ), and green (ε). JN403 is colored gray with the atoms colored as follows: violet for N, red for O, light blue for F, and light gray for H^+. The labeled residues are conserved among interfaces except Leu109 in the ε and δ subunits, which correspond to α7 Val108, as well as Lys32, which is present only in the ε subunit. The interactions of JN403 with Trp149 and Tyr93 are also shown. Note that opposite the α−δ interface, there is no hydrogen bond between Trp149 and JN403 at the α−ε interface. In contrast, a hydrogen bond with Y93 is detected at α7 and at both muscle AChR subunit interfaces. Hydrogen bonds are shown with dashed lines and π−cation interactions with solid lines.

dx.doi.org/10.1021/bi4012572 | *Biochemistry* XXXX, XXX, XXX−XXX

interacts with the aromatic cage by cation−π interactions, whereas its lipophilic group interacts with the hydrophobic cavity (Figure 7A). The docking of JN403 at each muscle subunit interface (Figure 7B,C) is energetically favorable, and its orientation is similar to that for the $\alpha7-\alpha7$ interface (Figure 7A). In particular, the quaternary amine is oriented toward the lower part of the cleft that contains the aromatic cage (Figure 7B,C). The positively charged group can form the typical cation−π interaction with the indole group of W149 (at loop B), whereas a hydrogen bond is formed with Y93 (at loop A) as described for the $\alpha7$ AChR.[9] JN403 can bridge the principal and complementary faces by interacting with Y190 and C192−193 (loop C, principal face) and W55 (loop D, complementary face). A remarkable difference in the binding of JN403 to each muscle AChR orthosteric site with respect to the $\alpha7$ orthosteric site is the probability of forming a hydrogen bond with W149. This hydrogen bond between the nitrogen atom of the carbamate group (NH) from JN403 and the oxygen atom from W149 is observed in the $\alpha7$ binding site (Figure 7A)[9] and in 70% of the docking runs at the $\alpha-\delta$ interface (Figure 7B). However, such a hydrogen bond is not detected at the $\alpha-\varepsilon$ interface (Figure 7C).

As in $\alpha7$, the aromatic ring of JN403 can interact with the hydrophobic cavity found in each muscle subunit interface (Figure 7). The calculated distances between the aromatic ring of JN403 and the side chains of ε-Leu109 and δ-Leu119 are shorter than 4.4 Å, supporting the possibility of forming hydrophobic contacts. It has been suggested that positively charged residues surrounding the binding cavity present in the $\alpha3\beta4$ AChR preclude the binding of JN403.[9] Along the same lines, the positively charged residue ε-Lys32 is also present in the $\alpha-\varepsilon$ interface (Figure 7C).

DISCUSSION

In this work, we reveal important differences in the functional and structural interaction of JN403 between the neuronal $\alpha7$ and muscle AChRs, thus providing further insights into the mechanisms underlying receptor selectivity.

Single-channel recordings indicate that JN403 is a low-efficacy partial agonist of adult muscle AChRs: it has low potency for activation, produces open-channel blockade, and enhances desensitization. These activities, which take place via the binding to both orthosteric and noncompetitive sites, make JN403 behave as an antagonist of adult and embryonic muscle AChRs, as observed in Ca^{2+} influx experiments. The weak agonistic efficacy of JN403 at muscle AChRs is supported by the observation that this drug activates AChR channels at concentrations ~20-fold higher than that for ACh (1 μM instead of 50 nM for ACh),[27] it elicits very infrequent and brief openings, and it does not produce clusters at any concentration, in contrast to what is observed with ACh.

In agreement with the weak agonism observed in the patch-clamp recordings and the weak antagonistic activity determined by Ca^{2+} influx experiments (Table 1), [^{3}H]cytisine competition binding experiments in the desensitized state revealed the low affinity of JN403 for muscle *Torpedo* AChR agonist sites (Table 2). Comparing our results with the binding affinity of JN403 for other AChR subtypes,[8,9] we found the following order of receptor selectivity: $\alpha7$ (55−200 nM) > $\alpha3\beta4$ (2.2−6.3 μM) > $\alpha4\beta2$ (28−158 μM) > $\alpha\beta\gamma\delta$ (112 μM in the desensitized state). These K_i values indicate that JN403 is at least 11−790 times more selective for the $\alpha7$ AChR than for other AChR subtypes.

Although speculative, molecular docking studies are valuable for providing experimentally testable hypotheses to further characterize agonist−receptor interactions. Our results show that JN403 has the potential to make the typical cation−π interactions with W149 and other aromatic residues at both muscle AChR subunit interfaces (Figure 7B,C). However, the hydrogen bond between the agonist and W149, which is required for potent activation of AChRs,[28,29] and has been shown in the $\alpha7$−JN403 complex,[9] is detected only at the $\alpha-\delta$ interface (Figure 7B). In addition, our docking studies show that positively charged residues near the binding cavity at the $\alpha-\varepsilon$ interface may impair ligand interaction as described for the $\alpha3\beta4$ AChR sites.[9] In agreement with the docking results, our single-channel recordings from $\alpha\beta\delta$ AChRs show that JN403 can activate these receptors through the $\alpha-\delta$ interface. Single-channel openings from ε-lacking AChRs activated by JN403 are more frequent and significantly more prolonged than those from wild-type AChR, as observed for ACh, thus indicating that JN403 activates muscle AChRs through the $\alpha-\delta$ interface. Unfortunately, activation through the $\alpha-\varepsilon$ interface cannot be experimentally evaluated because functional receptors are not expressed.[13]

The decrease in the duration of ACh-activated clusters of muscle AChRs without changes in the mean open time suggests an increased level of desensitization.[30] This is observed at very low concentrations (1 μM) where blockade is still not evident, indicating a higher potency for enhancing desensitization than for blocking. Although there are slight quantitative differences, probably due to the different methodologies, the increased level of desensitization elicited by JN403 detected from single-channel recordings is supported by the [^{3}H]cytisine and [^{3}H]TCP binding results indicating that JN403 enhances the binding of the radioligand to AChRs in the resting state by inducing AChR desensitization with apparent EC_{50} values of ~23−35 μM (Table 2). Benzylidene-anabaseine analogues, selective partial agonists of $\alpha7$ AChRs, also enhance the binding of [^{3}H]TCP to resting *Torpedo* AChRs[31] but with desensitizing potencies (apparent EC_{50} values of 0.2−3.9 μM) higher than that for JN403. The concentration range for the affinity of binding of JN403 to the TCP binding site in the desensitized state (~260 μM) is relatively higher than that for its desensitizing activity (35 μM) (Table 2), indicating that the TCP site is not responsible for the observed JN403-induced AChR desensitization. This result contrasts with the observed correlation between the binding affinities of other noncompetitive antagonists and their desensitizing potencies.[11,32] In this regard, other luminal and nonluminal sites[11,12,33] (reviewed in refs 5 and 34), different from that for TCP, could be more relevant for the observed desensitizing activity elicited by JN403.

Single-channel recordings show that JN403 produces significant open-channel blockade at concentrations of >10 μM, which is evidenced by the reduction of the mean open time of ACh-elicited events as a function of concentration. Because open-channel blockade can be produced by the interaction of the ligand with a luminal site, [^{3}H]TCP binding experiments were performed in an attempt to identify such a site. The results showing that JN403 enhances binding of [^{3}H]TCP to resting AChRs suggest that JN403 does not bind to this site, at least in this conformational state. In addition, JN403 inhibits binding of [^{3}H]TCP to desensitized AChRs with a very low affinity (Table 2). Although this latter result may suggest that TCP is not the blocking site, it cannot be ruled out because open-channel blockade occurs when the channel is in the open

dx.doi.org/10.1021/bi4012572 | *Biochemistry* XXXX, XXX, XXX−XXX

state and there is no structural information about the TCP binding site in this conformational state.

In this work, we show for the first time single channels from α7 AChRs activated by JN403. Our results reveal that the activation kinetics is very similar to that for ACh.[27] However, JN403 activates α7 AChRs at concentrations >1000-fold lower than that for ACh activation, indicating that JN403 is significantly more potent than the endogenous neurotransmitter. At higher concentrations ($\geq$10 μM), JN403 may also act as an open-channel blocker of α7 AChRs, as evidenced by the reduction in the mean open time. Alternatively, because desensitization may terminate α7 AChR channel openings,[27] such reduction may be mediated by an increased level of desensitization. The combination of open-channel blockade and an increased level of desensitization may account for the partial agonistic activity mediated by JN403 on the α7 AChR. Nevertheless, our study shows that very low concentrations of JN403, below the blocking ones, produce important activation of α7 without affecting other AChR subtypes.

Collectively, our results indicate that JN403 activates α7 AChRs with high potency and selectivity compared to those for muscle AChRs where it behaves as a very low-affinity partial agonist. By binding to noncompetitive sites, JN403 also produces an increased level of desensitization and open-channel blockade, which reduces even more muscle AChR responses. All three mechanisms make JN403 behave as an antagonist of muscle AChRs. The observed high selectivity for the α7 AChR might be important for the development of future therapies for Alzheimer's disease, schizophrenia, and wound healing where this receptor subtype has been found to play key roles.

AUTHOR INFORMATION

Corresponding Authors

*Department of Medical Education, California Northstate University College of Medicine, 9700 W. Taron Dr., Elk Grove, CA 95757. E-mail: hugo.arias@cnucom.org. Telephone: (916) 686-7300. Fax: (916) 686-7310.

*Instituto de Investigaciones Bioquímicas de Bahía Blanca, Camino La Carrindanga Km 7, 8000 Bahía Blanca, Argentina. E-mail: inbouzat@criba.edu.ar. Telephone: (54)291-4861201.

Funding

This research was supported by grants from ANPCyT, UNS, and CONICET (to C.B.).

Notes

The authors declare no competing financial interest.

ACKNOWLEDGMENTS

We thank the National Institute on Drug Abuse for the gift of phencyclidine.

ABBREVIATIONS

AChR, nicotinic acetylcholine receptor; JN403, (*S*)-(1-azabicyclo[2.2.2]oct-3-yl)carbamic acid (*S*)-1-(2-fluorophenyl)-ethyl ester; CCh, carbamylcholine; ACh, acetylcholine; FBS, fetal bovine serum; K_i, inhibition constant; K_d, dissociation constant; IC_{50}, ligand concentration that produces 50% inhibition (of binding or of agonist activation); n_H, Hill coefficient; EC_{50}, agonist concentration that produces 50% AChR activation; apparent EC_{50}, agonist concentration that produces 50% AChR desensitization.

REFERENCES

(1) Arias, H. R. (2006) Ligand-gated ion channel receptor superfamilies. In *Biological and Biophysical Aspects of Ligand-Gated Ion Channel Receptor Superfamilies* (Arias, H. R., Ed.) pp 1–25, Research Signpost, Kerala, India.

(2) Albuquerque, E. X., Pereira, E. F. R., Alkondon, A., and Rogers, S. W. (2009) Mammalian nicotinic acetylcholine receptors: From structure to function. *Physiol. Rev. 89*, 73–120.

(3) Romanelli, M. N., Gratteri, P., Guandalini, L., Martini, E., Bonaccini, C., and Gualtieri, F. (2007) Central nicotinic receptors: Structure, function, ligands, and therapeutic potential. *ChemMedChem. 2*, 746–767.

(4) Bartos, M., Corradi, J., and Bouzat, C. (2009) Structural basis of activation of Cys-loop receptors: The extracellular–transmembrane interface as a coupling region. *Mol. Neurobiol. 40*, 236–252.

(5) Arias, H. R., and Bouzat, C. (2010) Activation and modulation of the nicotine receptor. *Journal of Pediatric Biochemistry 1*, 53–73.

(6) Bouzat, C. (2012) New insights into the structural bases of activation of Cys-loop receptors. *J. Physiol. (Paris) 106*, 23–33.

(7) Mousa, S. A., and Arias, H. R. (2010) Angiogenesis modulation by nicotine and nicotinic ligands. *Journal of Pediatric Biochemistry 1*, 91–104.

(8) Feuerbach, D., Nozulak, J., Lingenhoehl, K., McAllister, K., and Hoyer, D. (2007) *Neurosci. Lett. 416*, 61–65.

(9) Arias, H. R., Gu, H., Feuerbach, D., and Wei, D.-Q. (2010) Different interaction between the agonist JN403 and the competitive antagonist methyllycaconitine with the human α7 nicotinic receptor. *Biochemistry 49*, 4169–4180.

(10) Feuerbach, D., Lingenhoehl, K., Olpe, H. R., Vassout, A., Gentsch, C., Chaperon, F., Nozulak, J., Enz, A., Bilbe, G., McAllister, K., and Hoyer, D. (2009) The selective nicotinic acetylcholine receptor α7 agonist JN403 is active in animal models of cognition, sensory gating, epilepsy and pain. *Neuropharmacology 56*, 254–263.

(11) Arias, H. R., Feuerbach, D., Targowska-Duda, K. M., Aggarwal, S., Lapinsky, D. J., and Jozwiak, K. (2012) Structural and functional interaction of (±)-2-(*N*-*tert*-butylamino)-3′-iodo-4′-azidopropiophenone, a photoreactive bupropion derivative, with nicotinic acetylcholine receptors. *Int. Neurochem. 61*, 1433–1441.

(12) Arias, H. R., Feuerbach, D., Bhumireddy, P., and Ortells, M. O. (2010) Inhibitory mechanisms and binding site locations for serotonin selective reuptake inhibitors on nicotinic acetylcholine receptors. *Int. J. Biochem. Cell Biol. 42*, 712–724.

(13) Bouzat, C., Bren, N., and Sine, S. M. (1994) Structural basis of the different gating kinetics of fetal and adult acetylcholine receptors. *Neuron 13*, 1395–1402.

(14) Bouzat, C., Barrantes, F., and Sine, S. (2000) Nicotinic receptor fourth transmembrane domain: Hydrogen bonding by conserved threonine contributes to channel gating kinetics. *J. Gen. Physiol. 115*, 663–672.

(15) Bouzat, C., Gumilar, F., del Carmen, E. M., and Sine, S. M. (2002) Subunit-selective contribution to channel gating of the M4 domain of the nicotinic receptor. *Biophys. J. 82*, 1920–1929.

(16) Williams, M. E., Burton, B., Urrutia, A., Shcherbatko, A., Chavez-Noriega, L. E., Cohen, C. J., and Aiyar, J. (2005) Ric-3 promotes functional expression of the nicotinic acetylcholine receptor α7 subunit in mammalian cells. *J. Biol. Chem. 280*, 1257–1263.

(17) Hamill, O. P., Marty, A., Neher, E., Sakmann, B., and Sigworth, F. J. (1981) Improved patch-clamp techniques for high-resolution current recording from cells and cell-free membrane patches. *Pfluegers Arch. 391*, 85–100.

(18) Goldstein, A., and Barrett, R. W. (1986) Ligand dissociation constants from competition binding assays: Errors associated with ligand depletion. *Mol. Pharmacol. 31*, 603–609.

(19) Pagán, O. R., Eterović, V. A., García, M., Vergne, D., Basilio, C. M., Rodríguez, A. D., and Hann, R. M. (2001) Cembranoid and long-chain alkanol sites on the nicotinic acetylcholine receptor and their allosteric interaction. *Biochemistry 40*, 11121–11130.

649 (20) Sali, A., Potterton, L., Yuan, F., van Vlijmen, H., and Karplus, M.
650 (1995) Evaluation of comparative protein modeling by MODELLER.
651 *Proteins 23*, 318−326.
652 (21) Hernando, G., Bergé, I., Rayes, D., and Bouzat, C. (2012)
653 Contribution of subunits to *Caenorhabditis elegans* levamisole-sensitive
654 nicotinic receptor function. *Mol. Pharmacol. 82*, 550−560.
655 (22) Morris, G., Goodsell, D. S., Halliday, R. S., Huey, R., Hart, W.
656 E., Belew, R. K., and Olson, A. J. (1998) Automated docking using a
657 Lamarckian genetic algorithm and empirical binding free energy
658 function. *J. Comput. Chem. 19*, 1639−1662.
659 (23) Arias, H. R., Bhumireddy, P., and Bouzat, C. (2006) Molecular
660 mechanisms and binding site locations for noncompetitive antagonists
661 of nicotinic acetylcholine receptors. *Int. J. Biochem. Cell Biol. 38*, 1254−
662 1276.
663 (24) Arias, H. R., Trudell, J. R., Bayer, E. Z., Hester, B., McCardy, E.
664 A., and Blanton, M. B. (2003) Noncompetitive antagonist binding sites
665 in the *Torpedo* nicotinic acetylcholine receptor ion channel. Structure-
666 activity relationship studies using adamantane derivatives. *Biochemistry*
667 *42*, 7358−7370.
668 (25) Auerbach, A., and Akk, G. (1998) Desensitization of mouse
669 nicotinic acetylcholine receptor channels. A two-gate mechanism. *J.*
670 *Gen. Physiol. 112*, 181−197.
671 (26) Bouzat, C., Bartos, M., Corradi, J., and Sine, S. M. (2008) The
672 interface between extracellular and transmembrane domains of
673 homomeric Cys-loop receptors governs open-channel lifetime and
674 rate of desensitization. *J. Neurosci. 28*, 7808−7819.
675 (27) Spitzmaul, G., Corradi, J., and Bouzat, C. (2004) Mechanistic
676 contributions of residues in the M1 transmembrane domain of the
677 nicotinic receptor to channel gating. *Mol. Membr. Biol. 21*, 39−50.
678 (28) Hibbs, R. E., Sulzenbacher, G., Shi, J., Talley, T. T., Conrod, S.,
679 Kem, W. R., Taylor, P., Marchot, P., and Bourne, Y. (2009) Structural
680 determinants for interaction of partial agonists with acetylcholine
681 binding protein and neuronal α7 nicotinic acetylcholine receptor.
682 *EMBO J. 28*, 3040−3051.
683 (29) Xiu, X., Puskar, N. L., Shanata, J. A. P., Lester, H. A., and
684 Dougherty, D. A. (2009) Nicotine binding to brain receptors requires
685 a strong cation-π interaction. *Nature 458*, 534−538.
686 (30) Gumilar, F., Arias, H. R., Spitzmaul, G., and Bouzat, C. (2003)
687 Molecular mechanisms of inhibition of nicotinic acetylcholine
688 receptors by tricyclic antidepressants. *Neuropharmacology 45*, 964−
689 976.
690 (31) Arias, H. R., Xing, H., MacDougall, K., Blanton, M. P., Soti, F.,
691 and Kem, W. R. (2009) Interaction of benzylidene-anabaseine
692 analogues with agonist and allosteric sites on muscle nicotinic
693 acetylcholine receptors. *Br. J. Pharmacol. 157*, 320−330.
694 (32) Arias, H. R., Feuerbach, D., Targowska-Duda, K. M., and
695 Jozwiak, K. (2011) Structure-activity relationship of ibogaine analogs
696 interacting at nicotinic acetylcholine receptors in different conforma-
697 tional states. *Int. J. Biochem. Cell Biol. 43*, 1330−1339.
698 (33) Arias, H. R., Fedorov, N. B., Benson, L. C., Lippiello, P., Gatto,
699 G. J., Feuerbach, D., and Ortells, M. O. (2013) Functional and
700 structural interaction of (−-)-reboxetine with the human $\alpha4\beta2$
701 nicotinic acetylcholine receptor. *J. Pharmacol. Exp. Ther. 344*, 113−
702 123.
703 (34) Arias, H. R. (2011) Allosteric modulation of nicotine
704 acetylcholine receptors. In *Pharmacology of Nicotinic Acetylcholine*
705 *Receptors from the Basic and Therapeutic Perspectives* (Arias, H. R., Ed.)
706 pp 151−173, Research Signpost, Kerala, India.